

Article

An Improved Underwater Electric Field-Based Target Localization Combining Subspace Scanning Algorithm And Meta-EP PSO Algorithm

Wenjing Shang ¹, Wei Xue ¹, Yingsong Li ^{1,2}, Xiangshang Wu ³ and Yidong Xu ^{1,*}

¹ College of Information and Communication Engineering, Harbin Engineering University, Harbin 150001, China; shangwenjing@hrbeu.edu.cn (W.S.); xuwei@hrbeu.edu.cn (W.X.); liyingsong@hrbeu.edu.cn (Y.L.)

² National Space Science Center, Chinese Academy of Sciences, Beijing 100190, China

³ Shanghai Mechanical & Electrical Engineering Research Institute, Shanghai 201109, China; wuxiangshang@foxmail.com

* Correspondence: xuyidong@hrbeu.edu.cn; Tel.: +86-132-6350-7375

Received: 13 February 2020; Accepted: 23 March 2020; Published: 26 March 2020

Abstract: In this paper, we propose an improved three-dimensional underwater electric field-based target localization method. This method combines the subspace scanning algorithm and the meta evolutionary programming (meta-EP) particle swarm optimization (PSO) algorithm. The subspace scanning algorithm is applied as the evaluation function of the electric field-based underwater target locating problem. The meta-EP PSO method is used to select M elite particles by the q-tournament selection method, which could effectively reduce the computational complexity of the three-dimensional underwater target localization. Moreover, the proposed meta-EP PSO optimization algorithm can avoid subspace scanning trapping into local minima. We also analyze the positioning performance of the uniform circular and cross-shaped electrodes arrays by using the subspace scanning algorithm combined with meta-EP PSO. According to the simulation, the calculation amount of the proposed algorithm is greatly reduced. Moreover, the positioning accuracy is effectively improved without changing the positioning accuracy and search speed.

Keywords: underwater localization; electric field; subspace scanning; meta-EP PSO

1. Introduction

Underwater target detection and estimation has a wide range of applications in marine salvage, marine exploration research, inspection of underwater facilities, underwater navigation and localization, and construction of an underwater environment [1–4]. However, due to the complexity of underwater environment, underwater target detection and estimation is still a challenging subject in theory and engineering practice [5–7]. In recent years, various underwater locating methods have been developed, including acoustic-, light-, and map-based locating methods [8–10]. At present, acoustic and optical imaging techniques are most commonly used in underwater target locating [11,12]. Acoustic signals have the advantage of less attenuation and longer underwater propagation distance than other methods. The underwater target positioning technology based on acoustic waves has provided a relatively complete theoretical system and has achieved considerable development [13,14]. However, the positioning performance of the acoustic method degrades due to specific factors, such as multipath effect, sonar scan angle, background noise, geomorphic structure complexity, and Doppler effect [15,16]. As the wavelength of the light is very short, the underwater positioning technology based on optical imaging has very high accuracy. Moreover, the situation is further complicated in shallow scenarios with rocks and sandbanks [17]. On the other hand, underwater imaging based on

optical imaging cannot work in turbid water or environments with no light [18]. On the contrary, the underwater target locating methods based on electromagnetic fields can avoid these drawbacks [19]. Besides, the electromagnetic field-based localization methods do not suffer from the Doppler effect due to velocity higher than that of the sound waves, and they do not require transparent water [20]. Therefore, the localization methods based on the electromagnetic field have received great attention. Generally, the electromagnetic noise is extremely low and stable, especially in deep ocean environments because of the high conductivity of seawater [21]. The electromagnetic wave-based locating methods and the low-frequency electro-locating methods are two primary types of underwater locating methods based on the electromagnetic field. In [20,22], the locating methods based on the power path loss model of an electromagnetic wave propagating through seawater were proposed. Because of a small skin depth of a high-frequency signal in seawater, the power of the radio-frequency signal decreases dramatically, which makes it unsuitable for wide-range locating. The locating methods based on the quasistatic electric field have been widely studied [1,7,23,24], because they have lower path losses in seawater compared to the methods based on the high-frequency electromagnetic signals. The electric sense locating methods based on bionics show good performance in underwater avoidance, docking, and close-range object shape estimation in dark and turbid environments. However, electric sense active locating methods are not suitable for long-distance target locating because the electric field re-emitted by the target is usually much weaker than that of the source field. In Peng's work [25], the underwater target electric field locating method based on the coupling Cole–Cole model and finite element method is proposed. To locate the underwater target, one should move the electrode array and acquire the voltage in different point, limiting the application of the locating system. The Multiple Signal Classification (MUSIC) algorithm is a noniterative algorithm that can be used to create a space spectrum to locate an underwater electromagnetic source. In [26], a MUSIC-type algorithm was proposed for locating small inclusions buried in a half-space by measuring the scattering amplitude at a fixed frequency in a two-dimensional space. The locating method was based on the far-field theory. However, the far-field theory is not suitable for underwater target locating because high-frequency radiation waves cannot be transferred to a long distance. Therefore, in this paper, underwater target locating based on the quasi-static electric field for near-distance locating is introduced.

In this paper, we introduce the mixed polarization MUSIC algorithm for underwater localization. The mixed polarization MUSIC algorithm is different from the other MUSIC algorithms for radar, such as root-MUSIC and beamspace MUSIC: MP-MUSIC could deal with signal polarization, which is suitable for underwater electro-locating, allowing us to get the space position of a electric dipole without considering or solving the moment azimuth of the electric dipole, reducing the computation time [27,28]. The position of the target can be located via finding the minimum eigenvalue of the estimated gain matrix and the project matrix of the noise subspace by using the MP-MUSIC algorithm [29]. Searching for the solution to the proposed MUSIC algorithms denotes an optimization problem, so using a suitable optimization method can significantly reduce the calculation time. The evolutionary programming with a meta evolutionary programming (meta-EP) mutation algorithm and the particle swarm optimization algorithm are combined to develop a hybrid particle swarm algorithm for three-dimensional underwater target positioning. The simulations are conducted to validate the effectiveness of the proposed localization algorithm at different electrode configurations. The simulation results show that the proposed meta-EP particle swarm optimization (PSO) hybrid algorithm for searching an optimal solution to the localization algorithm has strong competitiveness in terms of accuracy and convergence speed.

2. Underwater Target Electro-Locating Method

2.1. Underwater Electric Field Forward Model

The schematic of the three-dimensional multi-electrode underwater electric field positioning is shown in Figure 1. In Figure 1, the electric dipole source is located at position \mathbf{r}_p , so the potential of the i^{th} electrode can be calculated by

$$\varphi_{(i)} = k \frac{(\mathbf{r}_p - \mathbf{r}_i)^T \mathbf{p}}{|\mathbf{r}_p - \mathbf{r}_i|^3} = \mathbf{g}(i) \mathbf{p}, \quad (1)$$

where $k = u_0 / (4\pi)$ is a constant, \mathbf{p} is the dipole moment, \mathbf{r}_p is the location of electric dipole source, \mathbf{r}_i is the location of the i^{th} electrode, and $\mathbf{g}(i)$ is the gain vector of the i^{th} receiving electric dipole located at position \mathbf{r}_i .

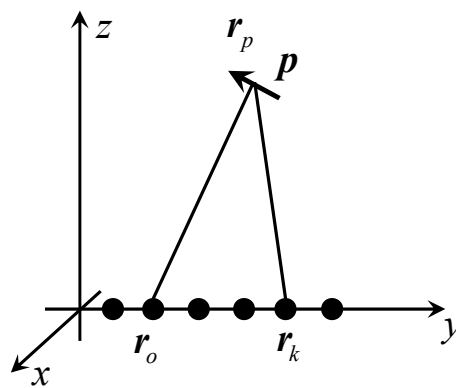


Figure 1. Schematic of the three-dimensional electric field-based multi-electrode underwater positioning.

The potential measured at different locations can be expressed as

$$\Psi = \begin{bmatrix} \varphi_1 \\ \vdots \\ \varphi_m \end{bmatrix} = k \begin{bmatrix} \vdots \end{bmatrix} \mathbf{p} = k \begin{bmatrix} \mathbf{g}(1) \\ \vdots \\ \mathbf{g}(m) \end{bmatrix} \mathbf{p} = \mathbf{G}(\mathbf{r}_p) \mathbf{p}, \quad (2)$$

where $\mathbf{G}(\mathbf{r}_p)$ denotes the gain matrix. According to (2), the potential Ψ is linearly proportional to the dipole moment \mathbf{p} . Location parameter \mathbf{r}_p in $\mathbf{G}(\mathbf{r}_p)$ is nonlinearly related to the potential Ψ . Each column in $\mathbf{G}(\mathbf{r}_p)$ represents different dipole components of the same position. Therefore, for p -dipoles, according to the superposition theorem, the receiving potential can be expressed in the matrix form as

$$\Psi = \begin{bmatrix} \mathbf{G}_1 & \cdots & \mathbf{G}_p \end{bmatrix} \begin{bmatrix} \mathbf{P}_1 \\ \vdots \\ \mathbf{P}_p \end{bmatrix}, \quad (3)$$

$$\mathbf{G}(\mathbf{r}) = \begin{bmatrix} \mathbf{G}_1 & \cdots & \mathbf{G}_p \end{bmatrix} = \begin{bmatrix} \mathbf{G}_1(\mathbf{r}_1) & \cdots & \mathbf{G}_p(\mathbf{r}_p) \end{bmatrix}, \quad (4)$$

$$\mathbf{T} = \begin{bmatrix} \mathbf{P}_1 \\ \vdots \\ \mathbf{P}_p \end{bmatrix}. \quad (5)$$

Equation (3) can be rewritten as $\Psi = \mathbf{G}(\mathbf{r}) \mathbf{T}$, where $\mathbf{G}_i(\mathbf{r}_i)$ denotes the gain matrix formulated by the i^{th} dipole located at position \mathbf{r}_i , the receiving potential Ψ is a column vector with a size of $m \times 1$, $\mathbf{G}(\mathbf{r})$ is a matrix with a size of $m \times 3p$, and \mathbf{T} is a column vector with a size of $3p \times 1$. Considering

that the current intensity of electric dipole changes with time and that its position does not change, Equation (5) can be rewritten as

$$\mathbf{T} = \begin{bmatrix} \mathbf{M}_1 \begin{bmatrix} \mathbf{S}_1(1) & \cdots & \mathbf{S}_1(n) \end{bmatrix} \\ \vdots \\ \mathbf{M}_p \begin{bmatrix} \mathbf{S}_p(1) & \cdots & \mathbf{S}_p(n) \end{bmatrix} \end{bmatrix} = \begin{bmatrix} \mathbf{M}_1 & & 0 \\ & \ddots & \\ 0 & & \mathbf{M}_p \end{bmatrix} \begin{bmatrix} \mathbf{S}_1(1) & \cdots & \mathbf{S}_1(n) \\ \vdots & \ddots & \vdots \\ \mathbf{S}_p(1) & \cdots & \mathbf{S}_p(n) \end{bmatrix}, \quad (6)$$

where \mathbf{M}_i represents the unit dipole moment of the i^{th} electric dipole and $\mathbf{S}_i(j)$ denotes the amplitude of the i^{th} electric dipole at time j . Therefore, Equation (3) can be expressed as

$$\begin{bmatrix} \varphi(1, 1) & \cdots & \varphi(1, n) \\ \vdots & \ddots & \vdots \\ \varphi(m, 1) & \cdots & \varphi(m, n) \end{bmatrix} = \begin{bmatrix} \mathbf{G}_1 & \cdots & \mathbf{G}_p \end{bmatrix} \begin{bmatrix} \mathbf{M}_1 & & 0 \\ & \ddots & \\ 0 & & \mathbf{M}_p \end{bmatrix} \begin{bmatrix} \mathbf{S}_1(1) & \cdots & \mathbf{S}_1(n) \\ \vdots & \ddots & \vdots \\ \mathbf{S}_p(1) & \cdots & \mathbf{S}_p(n) \end{bmatrix}. \quad (7)$$

Equation (7) can also be abbreviated as

$$\mathbf{\Psi} = \mathbf{GMS} = (\mathbf{GM})\mathbf{S} = \mathbf{HS}, \quad (8)$$

where \mathbf{G} consists of p electric dipoles with a unit dipole moment and m receiving electrodes array, which forms a $m \times 3p$ matrix. The $3p \times p$ diagonal matrix \mathbf{M} consists of p unit dipoles' moments with constant pointing. The dipole moment intensity matrix \mathbf{S} has a dimension of $p \times n$; $\mathbf{H} = [\mathbf{H}_1 \cdots \mathbf{H}_p] = \mathbf{GM}$, each column of \mathbf{H} contains all the information about an electric dipole.

The electric field positioning can be considered as solving the minimum problem defined by

$$\mathbf{J}_f(i) = \lambda_{\min}\{\mathbf{U}_{G_i}^T \mathbf{P}^\perp \mathbf{U}_{G_i}\}, \quad (9)$$

where $\lambda_{\min}\{\cdot\}$ denotes the minimum solution to the expression given in the curly brackets. Therefore, no special solution is required to make the minimum, and only the minimum eigenvalue related to the dipole moment needs to be calculated. The subspace scanning algorithm searches for possible locations of targets in a three-dimensional space. Accordingly, by finding the global minimum eigenvalue by eigenvalue decomposition, the target positioning in a three-dimensional space can be achieved.

2.2. Improved Three-Dimensional Subspace Scanning and Positioning Algorithm

In the three-dimensional underwater electric field-based target locating, it is necessary to obtain the received voltage data matrix using the receiving electrode array. The acquired data is given by

$$\mathbf{\Psi} = \mathbf{HS} + \mathbf{N}, \quad (10)$$

In Equation (10), the additive noise matrix \mathbf{N} is assumed to be zero mean with the covariance of $E\{\mathbf{NN}^T\} = \sigma_N^2 \mathbf{I}$, where $E\{\cdot\}$ denotes the expected value of the argument, \mathbf{H} denotes the gain matrix with a size of $(m < r)$, and \mathbf{S} denotes a matrix of a size $r \times n (r < n)$. The expected value of the matrix outer product $\mathbf{R}_{\Psi\Psi} = E\{\mathbf{\Psi\Psi}^T\}$ can be represented under the zero-mean white noise assumption as follows,

$$\mathbf{R}_{\Psi\Psi} = E\{[\mathbf{HS} + \mathbf{N}][\mathbf{HS} + \mathbf{N}]^T\} = \mathbf{HR}_S \mathbf{H}^T + \sigma_N^2 \mathbf{I}, \quad (11)$$

where $\mathbf{R}_S = E\{\mathbf{SS}^T\}$, and $\mathbf{R}_{\Psi\Psi}$ can be decomposed as

$$\mathbf{R}_{\Psi\Psi} = \mathbf{U}\mathbf{\Sigma}\mathbf{U}^T = \begin{bmatrix} \mathbf{U}_S & \mathbf{U}_N \end{bmatrix} \begin{bmatrix} \mathbf{\Sigma}_S & \\ & \mathbf{\Sigma}_N \end{bmatrix} \begin{bmatrix} \mathbf{U}_S & \mathbf{U}_N \end{bmatrix}^T. \quad (12)$$

In Equation (12), the signal subspace \mathbf{U}_S represents the vector space spanned by r eigenvectors corresponding to maximum eigenvalues. The remainder of $n - r$ eigenvector composes the noise subspace \mathbf{U}_N . Thus, Equation (9) can be rewritten as $\mathbf{J}_f(i) = \lambda_{\min} \left\{ \mathbf{U}_{G_i}^T \mathbf{U}_N \mathbf{U}_N^T \mathbf{U}_{G_i} \right\}$. The steps of the underwater target localization based on the subspace scanning algorithm are as follows.

- **Step 1:** Obtain measured voltage data using the receiving electrode array Ψ .
- **Step 2:** Use Equation (11) to construct the corresponding covariance matrix $\mathbf{R}_{\Psi\Psi}$.
- **Step 3:** Perform the eigenvalue decomposition on $\mathbf{R}_{\Psi\Psi}$, and calculate the orthogonal projection matrix of the signal subspace $\mathbf{P}^\perp = \mathbf{U}_N \mathbf{U}_N^T$.
- **Step 4:** Scan each possible point r_i in a three-dimensional positioning area, calculate its gain vector \mathbf{G}_i , perform the singular value decomposition (SVD) operation to obtain the corresponding value \mathbf{U}_{G_i} , evaluate each eigenvalue $\lambda_{\min}(\mathbf{U}_{G_i} \mathbf{P}^\perp \mathbf{U}_{G_i}^T)$, search first for the global minimum eigenvalue, and then the estimated point corresponding to the eigenvalue. The target position is estimated by the subspace scanning algorithm.

The proposed algorithm performs the eigenvalue decomposition operation on a gain matrix \mathbf{G}_i at each possible position in the space and evaluates the corresponding singular value during the target positioning process in a three-dimensional space. The positioning process is computationally expensive. Assume a three-dimensional space $1 \text{ m} \times 1 \text{ m} \times 1 \text{ m}$, where the positioning area is divided using a 1-cm grid. To complete the scanning and positioning processes, it is necessary to perform 1,000,000 SVD and eigenvalue decomposition operations and calculate the corresponding evaluation process which is meshgrid scanning method. In the case of the same hardware platform configuration, usually, a larger number of calculations means a longer calculation time, and the positioning speed is slower.

With the aim to reduce the number of calculations of the subspace scanning algorithm in the positioning process, an improved subspace scanning algorithm based on a multi-step search operation and a simplex algorithm is proposed which is multi-step scanning method. The steps of the proposed target location algorithm are as follows.

- **Step 1:** Obtain measured voltage data using the receiving electrode array Ψ .
- **Step 2:** Use Equation (11) to construct the corresponding covariance matrix $\mathbf{R}_{\Psi\Psi}$.
- **Step 3:** Perform the eigenvalue decomposition on $\mathbf{R}_{\Psi\Psi}$, and calculate the orthogonal projection matrix of the signal subspace $\mathbf{P}^\perp = \mathbf{U}_N \mathbf{U}_N^T$.
- **Step 4:** Scan each possible point r_i in a three-dimensional positioning area, calculate its gain vector \mathbf{G}_i , and perform the SVD operation to obtain the corresponding value \mathbf{U}_{G_i} , then evaluate each eigenvalue $\lambda_{\min}(\mathbf{U}_{G_i} \mathbf{P}^\perp \mathbf{U}_{G_i}^T)$, and search first for the global minimum eigenvalue, and then the estimated point corresponding to the eigenvalue. The target position is estimated by the subspace scanning algorithm.
- **Step 5:** Perform fine mesh division in the area near location r_{est} , and repeat **Step 4** to update the estimated location r_{est} .
- **Step 6:** Repeat **Step 5** until the predefined minimum grid size is reached, and output the corresponding result $r_{est-fin}$.
- **Step 7:** Use the simplex method to search for the initial point $r_{est-fin}$; the obtained position represents the final target position estimated by the improved algorithm.

The multi-step scanning method can effectively reduce the calculation burden and improve the positioning speed. Assume a three-dimensional space $1 \text{ m} \times 1 \text{ m} \times 1 \text{ m}$ again. Suppose a 5 cm low-resolution coarse grid global scan is adopted, the corresponding spatial points are used as a starting point to perform a local grid fine-grained search with a resolution of 2 cm, 1 cm, 0.5 cm, 0.2 cm, and 0.1 cm in turn. The simplex method is used to search the local area for the initial point to obtain the final target position. The total number of scans is $48,000 + N$ (simplex), where N (simplex) denotes the number of searches performed by the simplex method, and the average value of N (simplex)

of 100 is obtained by 1000 tests. Therefore, the multi-step scanning method for three-dimensional target positioning, compared with the meshgrid scanning method, can effectively reduce the number of calculations and can achieve positioning resolution of less than 0.1 cm. The multi-step scanning method can effectively increase the convergence speed, and thus improve the positioning speed.

In order to illustrate the effectiveness of the proposed positioning algorithm, assume that an electric dipole exists at the position (0.555, 0.555, 0.555) m with dipole moment orientation (1, 0, 0) A.m. A 100 Hz differential sine wave signal is loaded across the electric dipole. The uniform linear array, uniform circular array, and their modification array are commonly used in various applications [30,31]. The 8-channel uniform circular receiving electrodes with the circular radius R of 0.1 m are used for signal reception. The position information of the receiving electrodes is provided in Table 1, where electrode 9 that is at the center of the circle is set as a reference electrode, and the voltage is obtained by measuring the potential difference between it and other electrodes. The schematic diagram of the receiving electrode configuration is displayed in Figure 2. In Figure 2, the red dots represent the positive ends of the receiving electrodes, and the central black dot denotes the reference electrode. The received signal of electrode channels under the no-noise condition is presented in Figure 3.

The spatial spectrum image $L = 1/\lambda$ is drawn in the plane $(x, y, 0.555)$ m. According to the analysis of the proposed algorithm, the dipole localization problem can be transformed into the problem of finding the minimum generalized eigenvalue, which is equivalent to finding the maximum of L . The bright spot position in Figure 4 has the largest value, and the corresponding point coordinate set is (0.555, 0.555, 0.555) m that consists of the positions predicted by the proposed positioning algorithm. The simulation results show that the dipole position can be predicted better by the algorithm under the no-noise condition, and the simulation output is consistent with the actual position.

Table 1. Position of receiving electrodes for uniform circular electrode configuration (unit: m).

Electrode	1	2	3	4	5	6	7	8	9
x	0.1	0.0707	0	-0.070	-0.1	-0.070	0	0.070	0
y	0	-0.0707	-0.1	-0.070	0	0.070	0.1	0.070	0
z	0	0	0	0	0	0	0	0	0

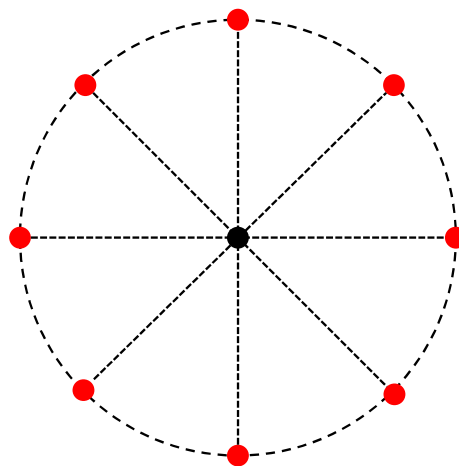


Figure 2. The uniform circular electrode configuration.

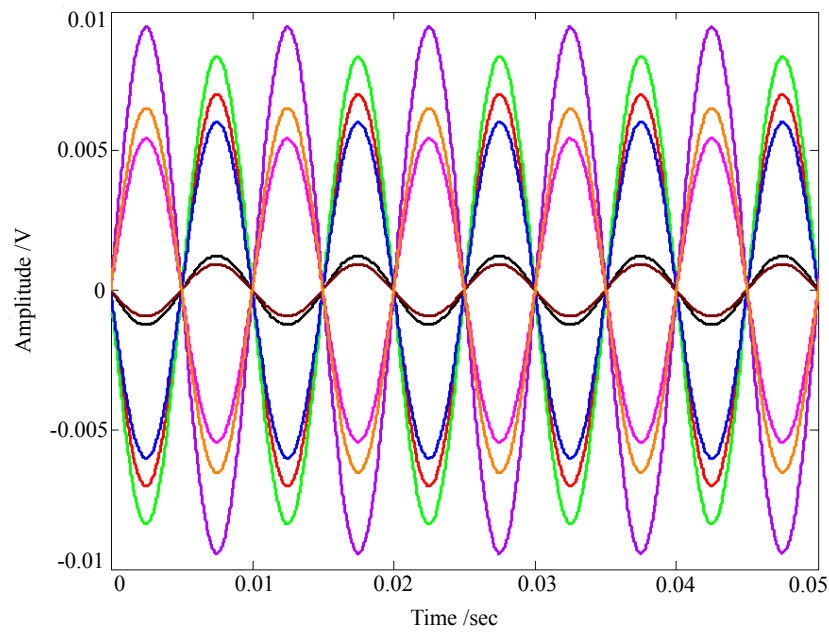


Figure 3. The received signal.

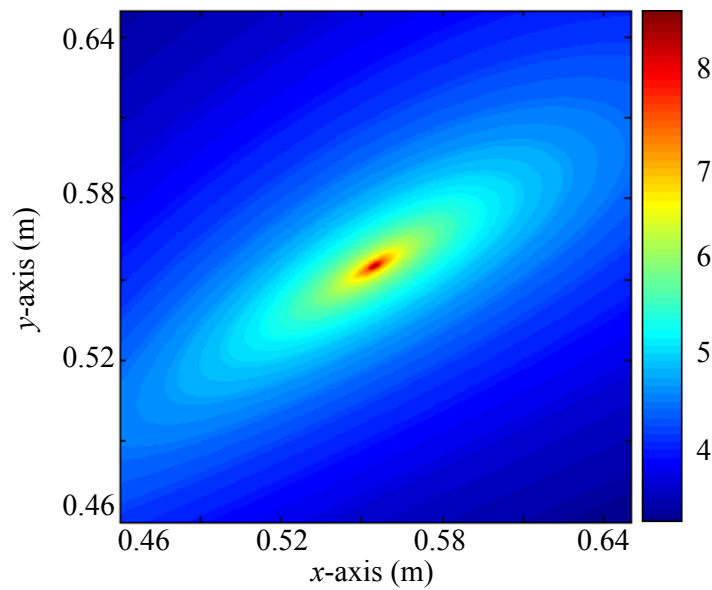


Figure 4. The spatial spectrum of in the plane $(x, y, 0.555)$ m.

2.3. Electro-Location Based on PSO Algorithm

Although a multi-step search operation can effectively improve the search speed, it has been found that this method can fall into local extremes when performing the localization tests on some points. The PSO is a populated search method that employs a swarm of particles to probe the search space [32]. The PSO solves a problem by finding a population of candidate solutions, here the dubbed particles, and moving these particles around in the search-space following simple mathematical formulae over the particle's position and velocity; therefore, the PSO is relatively fast, simple, and can easily converge to the optimal solution. Therefore, the dipole localization has been determined by implementing the improved PSO procedures. A detailed description of the implemented optimization algorithm for solving the dipole localization problems is herein provided. To test the ability of meta-EP PSO for underwater dipole localization, we conducted the simulation experiments and compared the proposed algorithm with other versions of the PSO algorithm.

1) Original PSO algorithm

Each particle is treated as a point in a D-dimensional space. Suppose the i^{th} particle is represented as $\mathbf{x}_i = (x_{i1}, x_{i2}, \dots, x_{iD})$. The change rate of the velocity of the i^{th} particle is represented as $\mathbf{v}_i = (v_{i1}, v_{i2}, \dots, v_{iD})$. In the PSO algorithm, initially, a population of particles is randomly generated. The population update rules of the PSO algorithm at every iteration step are described as follows,

$$\begin{cases} \mathbf{v}_i^{t+1} = \mathbf{v}_i^t + c_1 \text{Rand}() (\mathbf{p}_i - \mathbf{x}_i^t) + c_2 \text{Rand}() (\mathbf{p}_g - \mathbf{x}_i^t) \\ \mathbf{x}_i^{t+1} = \mathbf{x}_i^t + \mathbf{v}_i^{t+1} \end{cases}, \quad (13)$$

where c_1 and c_2 denote the constants of canonical PSO; t represents the time step; $\text{Rand}()$ stands for the random function in the range $[0, 1]$; and \mathbf{p}_i and \mathbf{p}_g denote the global best position and the personal best position of a particle, respectively.

2) Standard PSO (SPSO) algorithm

Shi and Eberhart [33] introduced an inertia weight w to improve the PSO accuracy by damping the velocities over time, allowing the swarm to converge with higher precision. By integrating w into the PSO algorithm, the velocity is updated by

$$\begin{cases} \mathbf{v}_i^{t+1} = w\mathbf{v}_i^t + c_1 \text{Rand}() (\mathbf{p}_i - \mathbf{x}_i^t) + c_2 \text{Rand}() (\mathbf{p}_g - \mathbf{x}_i^t) \\ \mathbf{x}_i^{t+1} = \mathbf{x}_i^t + \mathbf{v}_i^{t+1} \end{cases}, \quad (14)$$

A proper selection of the inertia weight ensures balance between the exploration and exploitation, where exploration represents the ability to test various regions in the problem space in order to achieve a good optimum, preferably the global one, and exploitation represents the ability to concentrate the search around a promising candidate solution in order to locate the optimum precisely. The choice of w defines how much the particle's current speed inherits. The more the particle inherits the current speed, the greater the global optimization ability, and the smaller the local search ability will be. Generally, fixed weight configuration and dynamic weight configuration are the two most common choices. According to the work in [32], the acceleration constants c_1 and c_2 can adjust and change the maximum step size of particles in time so that the particles can move in the direction of the best position of themselves. If the acceleration constants c_1 and c_2 are both equal to zero, the particles will move at the current speed until the boundary. In this case, the optimization process can be performed only in a limited range, which affects the algorithm performance. If the acceleration constant c_1 is set to be zero, it is a "social" model. The particles lack cognitive ability and rely only on the group experience. In this case, the algorithm converges quickly, but it can easily fall into a local optimum. On the other hand, when the acceleration constant c_2 is set to zero, it is a "cognitive" model. Particles cannot share socially, and rely only on their experience. In this case, it is difficult for the algorithm to find the global optimal value. Experiments have shown that there were no absolute optimal parameters, and it is necessary to determine appropriate parameters for each problem to obtain good convergence performance and robustness. Normally, the following values are used, $c_1 = c_2 = 2$ [32].

3) Proposed meta-EP PSO algorithm

As the underwater target locating represents a nonconvex optimization problem, the parameter selection for a specific problem is not straightforward. As mentioned previously, the PSO algorithm has a risk of trapping into local minima and losing the exploration-exploitation ability. Thus, to overcome these shortcomings, an improved PSO algorithm that combines the movement update of the property of the canonical PSO algorithm with the meta-EP mutation characteristic is proposed.

In the proposed algorithm, M particles are selected among the swarm population by the q -tournament selection method [34]. Then, the selected elite particles are evolved using the meta-EP mutation and q -tournament selection of the EP [35]. The meta-EP mutation can be expressed as

$$\begin{cases} \mathbf{x}'_i = \mathbf{x}_i + \sqrt{\sigma_i}N_i(0,1) \\ \sigma'_i = \sigma_i + \sqrt{\alpha}\sigma_iN_i(0,1) \end{cases} \quad (15)$$

where \mathbf{x}_i denotes the position and σ_i denotes the standard deviation of Gaussian mutations. A single offspring $(\mathbf{x}'_i, \sigma'_i)$ is generated by parent particle (\mathbf{x}_i, σ_i) , where $N_i(0,1)$ indicates that the random number is generated for each iteration; α denotes an exogenous parameter ensuring that σ_i tends to remain positive.

By evaluating the fitness value of particles, the global best position is determined. According to the global best position, the nearest elite position, the personal best position, velocity, and position of a particle are updated in the next iteration using the following relations,

$$\begin{cases} \mathbf{v}_i^{t+1} = w\mathbf{v}_i^t + c_p\text{Randp}()(\mathbf{p}_i - \mathbf{x}_i^t) + c_g\text{Randg}()(\mathbf{p}_g - \mathbf{x}_g^t) + c_n\text{Randn}()(\mathbf{p}_e - \mathbf{x}_g^t) \\ \mathbf{x}_i^{t+1} = \mathbf{x}_i^t + \mathbf{v}_i^{t+1} \end{cases} \quad (16)$$

where c_g , c_n , and c_p denote the constant of the global best, the constant of the nearest elite, and the constant of the personal best, respectively; $\text{Randp}()$, $\text{Randg}()$, $\text{Randn}()$ represent random functions in the range $[0, 1]$. The proposed meta-EP algorithm for searching the position of a target includes the following steps.

- Step 1:** Initialize the positions of N particles, and evaluate the fitness values of all the particles.
- Step 2:** Select M elite particles by the q -tournament selection method.
- Step 3:** Evolve the elite particles by the EP and Equation (15).
- Step 4:** Evaluate the fitness values of the particles and determine the global best position.
- Step 5:** Determine the global best position, the nearest elite position, and the personal best position, and update the velocity and position of a particle according to (16).
- Step 6:** If the termination conditions are not satisfied, go to **Step 2**; otherwise, output the global best position.

2.4. Proposed Meta-EP PSO Algorithm for Underwater Dipole Localization

In this paper, the improved three-dimension subspace scanning and proposed meta-EP PSO algorithm is applied to underwater target localization. First, the forward model, electrode configuration, parameters, and the fitness function of the PSO are determined.

The flowchart of the proposed localization algorithm is presented in Figure 5. One of the key issues in the proposed algorithm is finding a suitable mapping between the localization problem solution and the PSO particle. The proposed PSO algorithm is applied to searching the solution to $\lambda_{\min}(\mathbf{U}_{G_i}\mathbf{P}^\perp\mathbf{U}_{G_i}^\top)$. The dimension of the search space D , that is, the number of the elements of one particle, is equal to the number of position parameters of dipoles. For the source model with one dipole, D is equal to three, and a representation of dipole position is expressed as (x, y, z) . The individuals in the swarm are initialized by setting their positions and velocities randomly in the searching space. Then, the velocity and position of particles are updated in each iteration. The optimization iteration is terminated when the pre-defined maximum iteration number is reached.

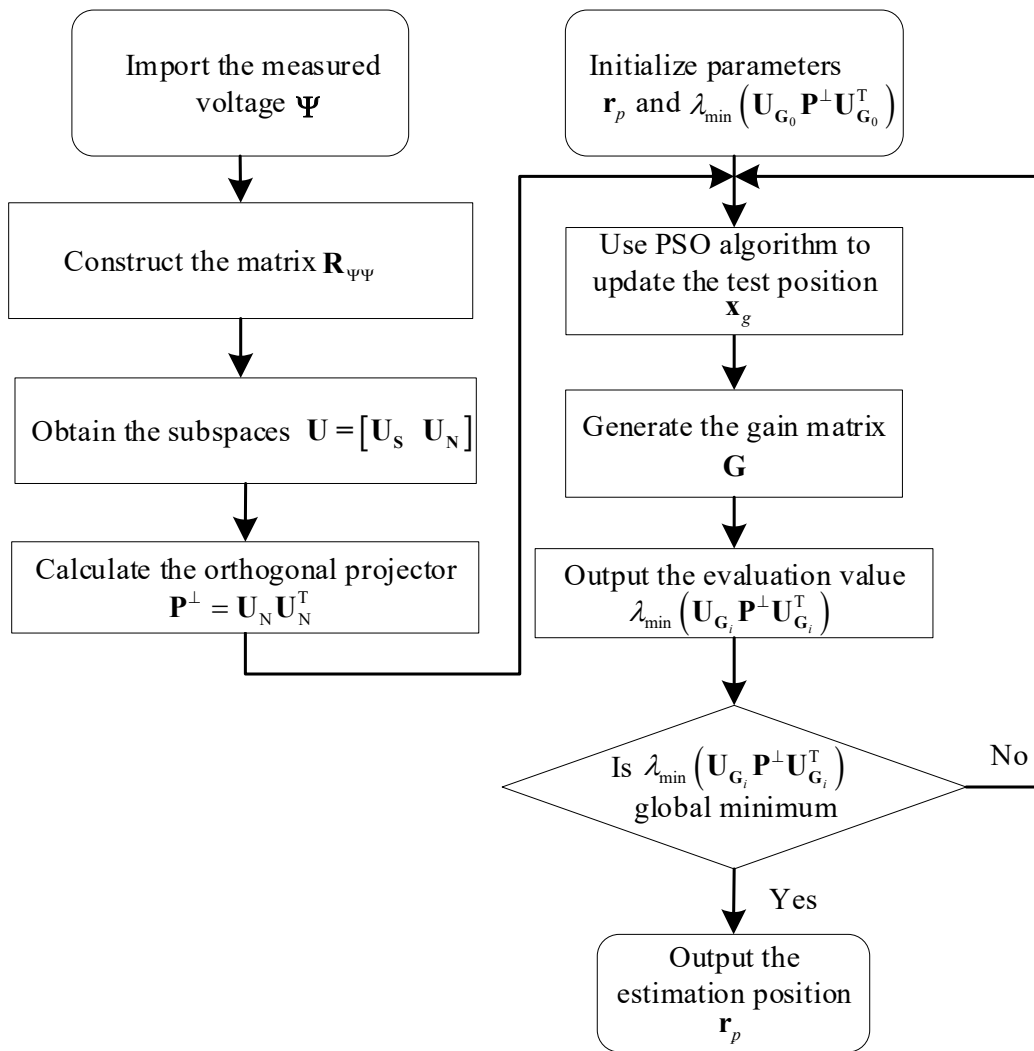


Figure 5. The flowchart of the proposed localization algorithm.

3. Numerical Simulations

In order to test the feasibility of the proposed PSO algorithm in the underwater target localizing, two simulation experiments were conducted to evaluate the positioning performance. The uniform circular electrode and cross electrode configurations are adopted as receiving electrode configurations. The schematic diagrams of the two common receiving electrode configurations are given in Figure 6a,b, where the red dots represent the positive receiving channels of the electrode channels, and the black dots represent the negative receiving channels of the electrode channels. In the two simulations, the radius R of the uniform circular receiving electrode was 0.1 m, and the electric dipole target was set in the plane xOy . The distance between the center of the receiving array and the target was r , and the electric dipole moment was $(1, 0, 0)$ m. At the signal-to-noise ratio of 40 dB, tests were performed 1000 times on each point, respectively, and the root mean square (RMS) error was calculated for each point at 0.5 m, 1 m, 2 m, 3 m, and 4 m, respectively.

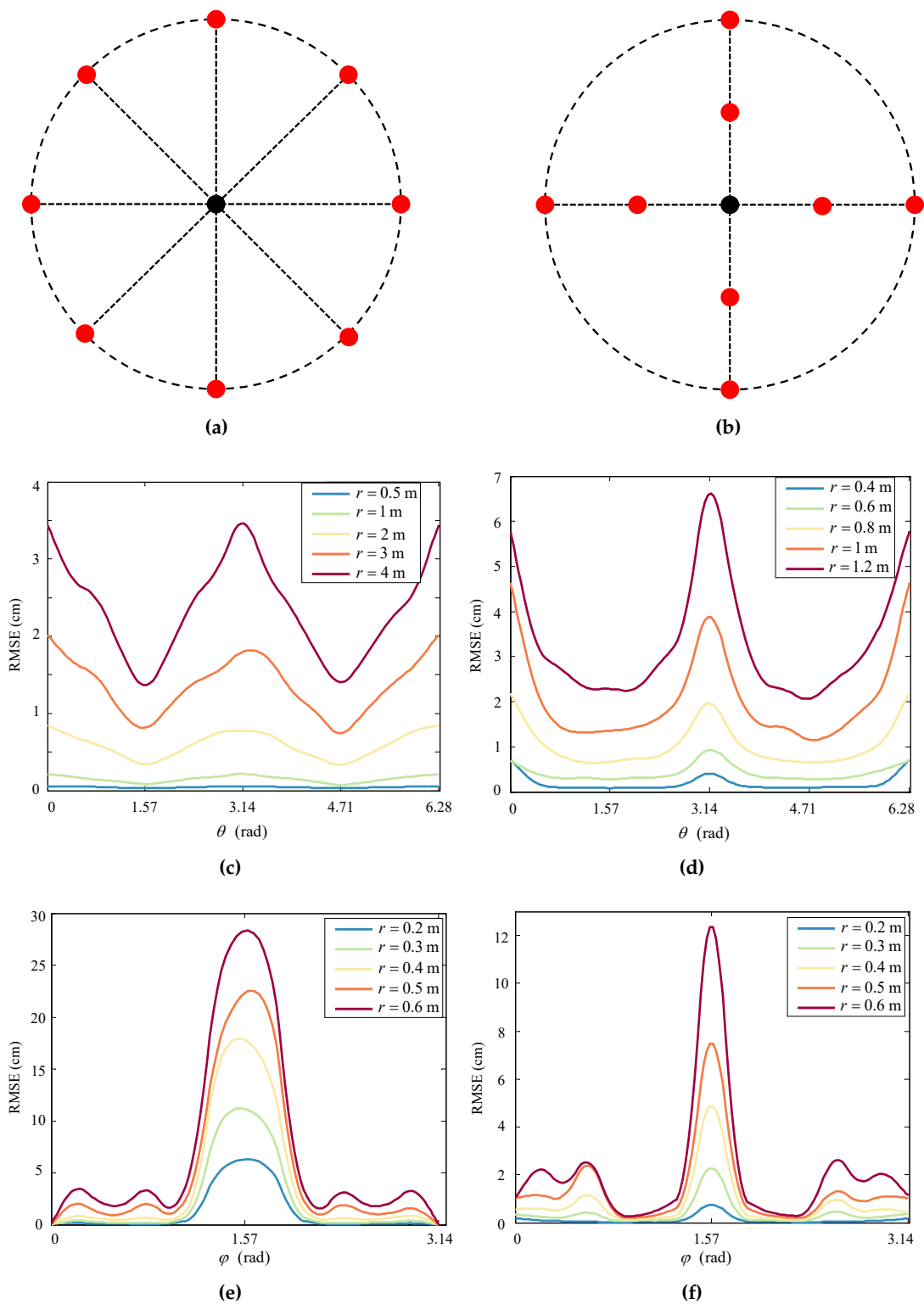


Figure 6. (a) The uniform circular electrode configuration; (b) The cross-shaped electrode configuration (c) Positioning error of uniform circular electrode configuration in the plane xOy; (d) Positioning error of the cross-shaped electrode configuration in the plane xOy; (e) Positioning error of uniform circular electrode configuration in the plane xOz; (f) Positioning error of the cross-shaped electrode configuration in the plane xOz.

3.1. Locating Performance of Uniform Circular Electrode Configuration

The electrode positions in the uniform circular receiving electrode configuration were the same as Table 1. The positioning performances at different positions in the planes xOy and plane xOz were studied, and the corresponding test results are shown in Figure 6c,e, respectively.

As presented in Figure 6c, (1) as the positioning distance increased in the plane xOy, the positioning error also increased; (2) at the same positioning distance r , the positioning error showed a certain regularity with the change in the deflection angle θ , namely, in the range of deflection angle from $(0, \pi/2)$ to $(\pi, 3\pi/2)$, the positioning error decreased with the deflection angle. On the other hand, in the range of the deflection angle from $(\pi/2, \pi)$ to $(3\pi/2, 2\pi)$, the positioning error increased with the deflection angle; (3) the locating system had blind points at the deflection angle of zero and π due to the symmetry of acquainted data—the received electrode voltage values of channels 2, 3, and 4 were, respectively, equal to that of channels 8, 7, and 6. For all the other points, the difference in the received voltage between the electrodes was small.

Similarly, in the case of a uniform circular electrode configuration, the positioning performance at different positions in the plane xOz was also studied, and the results are shown in Figure 6e. As shown in Figure 6e, the blind points occur at the norm direction of plane xOz because the signal intensity received by electrode channels 3 and 7 was equal to zero, whereas the elevation angle was $\pi/2$. By comparing the results presented in Figure 6c with those presented in Figure 6e, it can be found that the uniform circular electrode configuration provided better locating performance in the plane xOy.

3.2. Locating Performance of Cross-Shape Electrode Configuration

In the cross-shaped receiving electrode configuration, the electrode positions were as given in Table 2. The positioning performance at different positions in the planes xOy and xOz were studied, and the results are shown in Figure 6d,f, respectively.

Table 2. Position of receiving electrodes for cross-shaped electrode configuration (unit: m).

Electrode	1	2	3	4	5	6	7	8	9
x	−0.1	−0.05	0.05	0.1	0	0	0	0	0
y	0	0	0	0	−0.1	−0.05	0.05	0.1	0
z	0	0	0	0	0	0	0	0	0

Based on the results presented in Figure 6d, a similar conclusion with that of the uniform circular electrode configuration in the plane xOy can be obtained. However, the cross-shaped electrode configuration showed worse locating performance in the plane xOy compared with the uniform circular electrode configuration. For instance, the minimum locating error of the cross-shaped electrode configuration was larger than 1.5 cm, whereas the maximum locating error of the uniform circular electrode configuration was less than 0.3 cm.

Similarly, the positioning performance of the cross-shaped receiving electrode configuration at different positions in the plane xOz was also studied. The test results are shown in Figure 6f. As can be seen in Figure 6f, the blind point occurred in the direction normal to the xOz plane. However, compared with the uniform circular electrode configuration, the cross-shaped electrode configuration provided better locating performance. By comparing the positioning performances of the uniform circular receiving electrode configuration and the cross-shaped receiving electrode configuration, the following conclusions were drawn.

- (1) For both the uniform circular receiving electrode configuration and the cross-shaped receiving electrode configuration, the positioning performance in the plane xOy was better than that in the plane xOz when the subspace scanning algorithm was used to locate underwater targets.
- (2) The positioning performance of the uniform circular receiving electrode configuration was better than that of the cross-shaped receiving electrode configuration in the plane xOy. Moreover,

the positioning performance of the cross-shaped receiving electrode configuration was better than that of the uniform circular receiving electrode configuration in the plane xOz.

- (3) Both configurations had certain positioning blind spots in the spatial three-dimensional positioning process.

4. Simulation and Analysis of the Proposed Algorithm

In this section, a simulation model and a detailed study of the proposed algorithm in underwater target locating are provided. The receiving array consisted of eight equidistant electrodes in the loop insulator framework. The positions of electrodes are shown in Table 1, and the radius of the loop insulator framework was 0.1 m. In the simulation, the dipole was placed at the position of (0.555, 0.555, 0.555) m with the current moment of (1, 0, 0) A·m.

The proposed meta-EP PSO algorithm was compared with the canonical PSO and SPSO algorithms. In order to ensure an objective comparison, the locating error was defined as

$$LE = \sqrt{(x_{est} - x_0)^2 + (y_{est} - y_0)^2 + (z_{est} - z_0)^2}, \tag{17}$$

where $(x_{est}, y_{est}, z_{est})$ denoted the position estimated by an algorithm, and (x_0, y_0, z_0) denoted the actual dipole position.

The configuration parameters of the PSO, SPSO, and meta-EP PSO algorithms are given in Table 3. According to [32], in the fixed-weight configuration, the inertia weight w is commonly in the interval [0.8, 1.2]. Therefore, the dynamic weight configuration was used, where gradually decreased from 0.9 to 0.4. Accordingly, particles had different development and exploration capabilities at different stages of evolution. In the comparison, the population size was set to 30 and $c_1 = c_2 = 2$.

Table 3. The configuration parameters of the PSO, SPSO, and meta-EP PSO algorithms.

Algorithm	w	c_1	c_2	c_3	Size
PSO	-	2	2	-	30
SPSO	0.9 ~ 0.4	2	2	-	30
meta-EP PSO	0.9 ~ 0.4	0.8	0.4	0.8	30

Table 4 gives the average test results for 100 tests with 200 iterations each. The locating error of one of the tests is presented in Figure 7, and the position estimation in each iteration of the meta-EP PSO algorithm is presented in Figure 8.

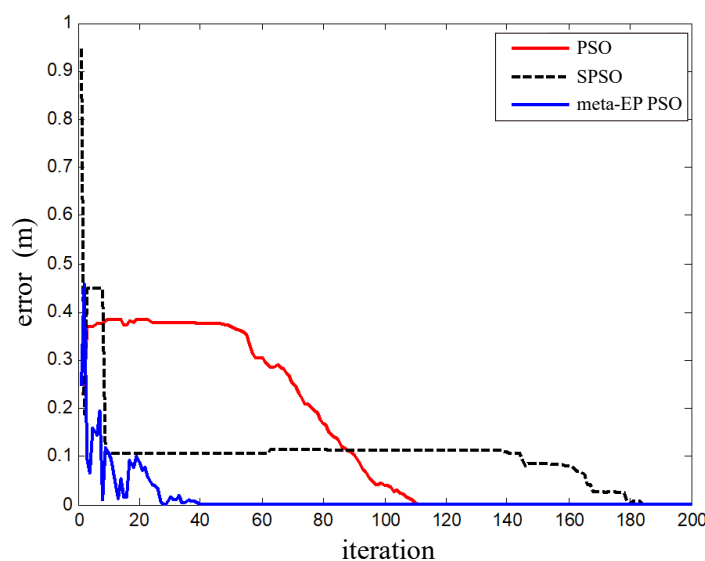


Figure 7. The locating error of one of the conducted tests.

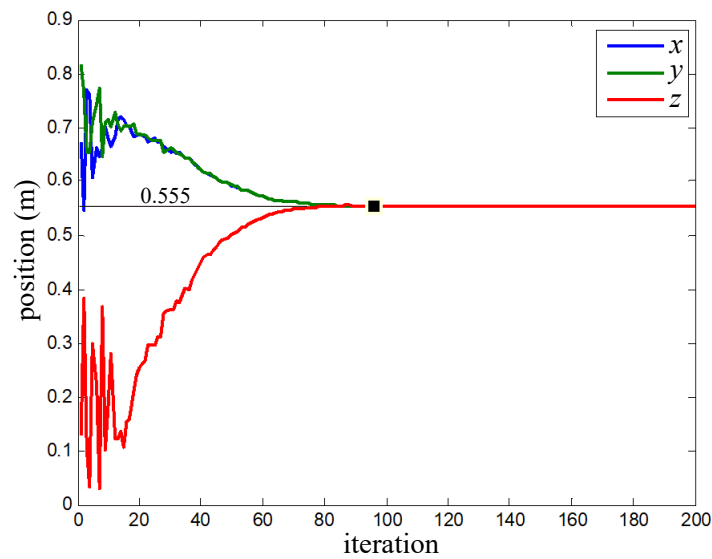


Figure 8. Position estimation in each iteration of the proposed meta-EP PSO algorithm.

Table 4. Test results of different algorithms.

Algorithm	PSO	SPSO	Meta-EP PSO
LE	0.545	0.356	0.006

As presented in Table 4, the PSO and SPSO algorithms converge to the local minimums during the positioning process, resulting in large positioning errors, which make them unsuitable for three-dimensional positioning scenarios. On the contrary, the proposed meta-EP PSO algorithm converged to the global minimum and provided the smallest positioning error among all the algorithms.

In order to study the computation of the meta-EP PSO further, we terminated the algorithm and recorded the number of iterations of the meta-EP PSO algorithm when the positioning error was less than 1 cm. The number of iterations of each test is shown in Figure 9.

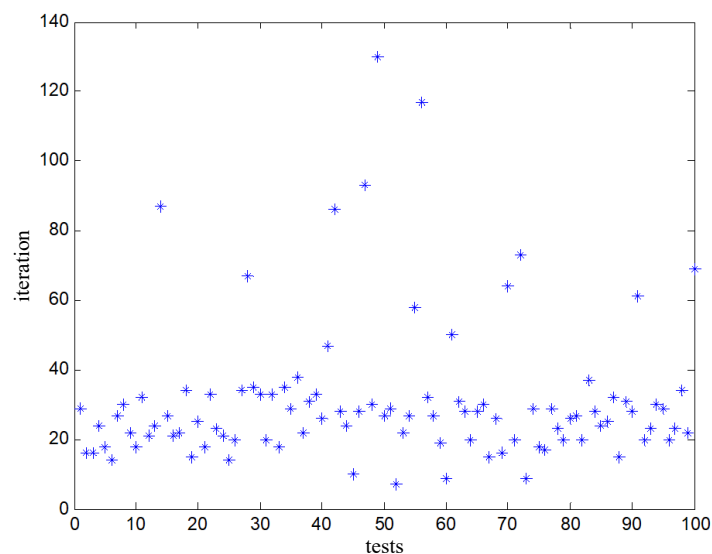


Figure 9. The number of iterations of each test.

As can be seen in Figure 9, most tests of the proposed algorithm terminated at up to 40 iterations. The average iteration number of the tests was 31.2, the maximum iteration number was 130,

and the minimum iteration number was 7. The evolution of the algorithm in one iteration required the evaluation of all the particles in the population and the children generation. In this paper, the population size was set to 30, and the number of elite particles was set to 3. Thus, each iteration required at least 33 evaluations. Therefore, the maximum number of evaluation tests was 4290, and the average number of evaluation test was 1031.25. The average computation of the meta-EP PSO, meshgrid scanning method and the multi-step scanning are given in Table 5. Compared with the meshgrid scanning method of 1,000,000 times, the calculation amount of the proposed algorithm was greatly reduced to only 0.103% of the meshgrid scanning method. Similarly, the computation burden of meta-EP PSO is 2.14% of the multi-step method. The positioning accuracy was effectively improved without changing the positioning accuracy and search speed.

Table 5. Comparison of different methods.

Method	Evaluations
Meta-EP PSO	1031.25
Meshgrid scanning	1,000,000
Multi-step scanning	48,100

5. Conclusions

In this paper, we study the target locating in the underwater environment based on the electric field. The subspace scanning algorithm is applied as the evaluation function of the electric field-based underwater target locating problem. To find the global minimum of the evaluation function, the meta-EP PSO optimization algorithm is proposed. The meta-EP PSO method selects M elite particles by the q -tournament selection method, which could significantly speed up the convergence and avoid subspace scanning trapping into local minima. According to our simulations, the meta-EP PSO calculation burden is 0.10% of the meshgrid scanning method and 2.14% of the multi-step scanning method. The simulations show the meta-EP PSO provides more accurate locating performance, where the root mean square locating error is 0.006 m far smaller than the PSO and SPSO. Moreover, the meta-EP PSO shows fewer convergence steps compared with the PSO and SPSO. It takes the meta-EP PSO less than 40 generations to converge, whereas it takes totally 110 generations for PSO and 185 generations for SPSO. We also study the influence of the electrodes array on the locating performance. The uniform circular and the cross-shaped electrodes arrays are constructed. According to the simulations, we found the uniform circular electrodes array has better locating performance than that of the cross-shaped electrodes array in the plane xOy . However, the cross-shaped electrodes array shows better locating performance in the plane xOz . In our future work, we will optimize the electrode configurations to obtain a better locating performance.

Author Contributions: W.S. did the mathematical modeling and the simulations. W.S. also wrote the draft of the paper. Y.X. and X.W. contributed to the revisions and the discussion of the results. W.X. and Y.L. put forward to the idea and checked the simulation of this paper. All authors have read and agreed to the published version of the manuscript.

Funding: This work was supported in part by the Fundamental Research Funds for the Central Universities under Grant 3072019CFJ0802, in part by the Free Inquiry Projects of Fundamental Research Funds for the Central Universities, in part by the Fundamental Research Funds for the Central Universities under Grant HEUCFG201829, in part by the China Postdoctoral Science Foundation under Grant 2018M631911, and in part by the Heilongjiang Postdoctoral Fund under Grant LBH-Z18055.

Conflicts of Interest: The authors declare no conflicts of interest.

References

1. Lebastard, V.; Boyer, F.; Lanneau, S. Reactive underwater object inspection based on artificial electric sense. *Bioinspiration Biomim.* **2016**, *11*, 045003. [[CrossRef](#)] [[PubMed](#)]
2. Burguera, A. A novel approach to register sonar data for underwater robot localization. In Proceedings of the 2017 Intelligent Systems Conference (IntelliSys), London, UK, 7–8 September 2017; pp. 1034–1043.
3. Ol'shanskii, V.; Pavlov, D.; Volkov, S.; El'yashev, D. Electric fishes as a biological prototype of new technology. *Her. Russ. Acad. Sci.* **2009**, *79*, 64–77. [[CrossRef](#)]
4. Peralta, G.; Bonin-Font, F.; Caiti, A. Real-time Hash-based Loop Closure Detection in Underwater Multi-Session Visual SLAM. In Proceedings of the OCEANS 2019-Marseille, Marseille, France, 17–20 June 2019; pp. 1–7.
5. Bazeille, S.; Lebastard, V.; Lanneau, S.; Boyer, F. Model based object localization and shape estimation using electric sense on underwater robots. *IFAC-PapersOnLine* **2017**, *50*, 5047–5054. [[CrossRef](#)]
6. Boyer, F.; Lebastard, V.; Chevallereau, C.; Servagent, N. Underwater reflex navigation in confined environment based on electric sense. *IEEE Trans. Robot.* **2013**, *29*, 945–956. [[CrossRef](#)]
7. Bai, Y.; Snyder, J.B.; Peshkin, M.; MacIver, M.A. Finding and identifying simple objects underwater with active electrosense. *Int. J. Robot. Res.* **2015**, *34*, 1255–1277. [[CrossRef](#)]
8. Carroll, P.; Zhou, S.; Zhou, H.; Xu, X.; Cui, J.H.; Willett, P. Underwater localization and tracking of physical systems. *J. Electr. Comput. Eng.* **2012**. [[CrossRef](#)]
9. Lefort, R.; Real, G.; Drémeau, A. Direct regressions for underwater acoustic source localization in fluctuating oceans. *Appl. Acoust.* **2017**, *116*, 303–310. [[CrossRef](#)]
10. Burguera, A. Cluster-based Scan Matching for Robust Motion Estimation and Loop Closing. In Proceedings of the 2019 IEEE International Conference on Systems, Man and Cybernetics (SMC), Bari, Italy, 6–9 October 2019; pp. 2512–2517.
11. Al_Aboosi, Y.; Sha'ameri, A.Z. Experimental Multipath Delay Profile of Underwater Acoustic Communication Channel in Shallow Water. *Indones. J. Electr. Eng. Comput. Sci.* **2016**, *2*, 351–358. [[CrossRef](#)]
12. Marani, G.; Choi, S.K. Underwater target localization. *IEEE Robot. Autom. Mag.* **2010**, *17*, 64–70. [[CrossRef](#)]
13. Huang, Z.; Xu, J.; Gong, Z.; Wang, H.; Yan, Y. Source localization using deep neural networks in a shallow water environment. *J. Acoust. Soc. Am.* **2018**, *143*, 2922–2932. [[CrossRef](#)]
14. Xu, Y.; Guo, L.; Shang, W.; Li, Y. Underwater electro-location method based on improved matrix adaptation evolution strategy. *IEEE Access* **2018**, *6*, 39220–39232. [[CrossRef](#)]
15. Esmail, H.; Jiang, D. Multicarrier communication for underwater acoustic channel. *Int. J. Commun. Netw. Syst. Sci.* **2013**, *6*, 361.
16. Ebihara, T.; Leus, G. Doppler-resilient orthogonal signal-division multiplexing for underwater acoustic communication. *IEEE J. Ocean. Eng.* **2015**, *41*, 408–427.
17. Negre, P.L.; Bonin-Font, F.; Oliver, G. Cluster-based loop closing detection for underwater slam in feature-poor regions. In Proceedings of the 2016 IEEE International Conference on Robotics and Automation (ICRA), Stockholm, Sweden, 16–21 May 2016; pp. 2589–2595.
18. White, E.M.; Partridge, J.C.; Church, S.C. Ultraviolet dermal reflexion and mate choice in the guppy, *Poecilia reticulata*. *Anim. Behav.* **2003**, *65*, 693–700. [[CrossRef](#)]
19. Zazo, J.; Macua, S.V.; Zazo, S.; Pérez, M.; Pérez-Álvarez, I.; Jiménez, E.; Cardona, L.; Brito, J.H.; Quevedo, E. Underwater electromagnetic sensor networks, part II: Localization and network simulations. *Sensors* **2016**, *16*, 2176. [[CrossRef](#)] [[PubMed](#)]
20. Park, D.; Kwak, K.; Kim, J.; Chung, W.K. Underwater sensor network using received signal strength of electromagnetic waves. In Proceedings of the 2015 IEEE/RSJ International Conference on Intelligent Robots and Systems (IROS), Hamburg, Germany, 28 September–2 October 2015; pp. 1052–1057.
21. Shang, W.; Xue, W.; Xu, Y.; Geng, W. Undersea Target Reconstruction Based on Coupled Laplacian-of-Gaussian and Minimum Gradient Support Regularizations. *IEEE Access* **2019**, *7*, 171633–171647. [[CrossRef](#)]
22. Duecker, D.A.; Geist, A.R.; Hengeler, M.; Kreuzer, E.; Pick, M.A.; Rausch, V.; Solowjow, E. Embedded spherical localization for micro underwater vehicles based on attenuation of electro-magnetic carrier signals. *Sensors* **2017**, *17*, 959. [[CrossRef](#)]

23. Wang, K.; Do, K.D.; Cui, L. An underwater electrosensor for identifying objects of similar volume and aspect ratio using convolutional neural network. In Proceedings of the 2017 IEEE/RSJ International Conference on Intelligent Robots and Systems (IROS), Vancouver, BC, Canada, 24–28 September 2017; pp. 4963–4968.
24. Wang, K.; Do, K.D.; Cui, L. Underwater active electrosense: A scattering formulation and its application. *IEEE Trans. Robot.* **2017**, *33*, 1233–1241. [[CrossRef](#)]
25. Peng, J.; Wu, J. A numerical simulation model of the induce polarization: Ideal electric field coupling system for underwater active electrolocation method. *IEEE Trans. Appl. Supercond.* **2016**, *26*, 1–5. [[CrossRef](#)]
26. Ammari, H.; Iakovleva, E.; Lesselier, D. A MUSIC algorithm for locating small inclusions buried in a half-space from the scattering amplitude at a fixed frequency. *Multiscale Model. Simul.* **2005**, *3*, 597–628. [[CrossRef](#)]
27. Shirmehnji, F.; Nezhad, A.Z.; Firouzeh, Z.H. Object locating in anisotropic dielectric background using MUSIC algorithm. In Proceedings of the 2016 8th International Symposium on Telecommunications (IST), Tehran, Iran, 27–28 September 2016; pp. 396–400.
28. Xu, Y.; Shang, W.; Guo, L.; Qi, J.; Li, Y.; Xue, W. Active electro-location of objects in the underwater environment based on the mixed polarization multiple signal classification algorithm. *Sensors* **2018**, *18*, 554. [[CrossRef](#)] [[PubMed](#)]
29. Shahbazi, F.; Ziehe, A.; Nolte, G. Self-Consistent MUSIC algorithm to localize multiple sources in acoustic imaging. In Proceedings of the 4th Berlin Beamforming Conference, Berlin, Germany, 22–23 February 2012; pp. 22–23.
30. Shi, W.; Li, Y.; Zhao, L.; Liu, X. Controllable sparse antenna array for adaptive beamforming. *IEEE Access* **2019**, *7*, 6412–6423. [[CrossRef](#)]
31. Zhang, X.; Jiang, T.; Li, Y.; Zakharov, Y. A novel block sparse reconstruction method for DOA estimation with unknown mutual coupling. *IEEE Commun. Lett.* **2019**, *23*, 1845–1848. [[CrossRef](#)]
32. Marini, F.; Walczak, B. Particle swarm optimization (PSO). A tutorial. *Chemom. Intell. Lab. Syst.* **2015**, *149*, 153–165. [[CrossRef](#)]
33. Shi, Y.; Eberhart, R.C. Parameter selection in particle swarm optimization. In Proceedings of the International Conference on Evolutionary Programming, San Diego, CA, USA, 25–27 March 1998; pp. 591–600.
34. Lee, K.B.; Kim, J.H. Particle swarm optimization driven by evolving elite group. In Proceedings of the 2009 IEEE Congress on Evolutionary Computation, Trondheim, Norway, 18–21 May 2009; pp. 2114–2119.
35. Fogel, D.B. An introduction to simulated evolutionary optimization. *IEEE Trans. Neural Netw.* **1994**, *5*, 3–14. [[CrossRef](#)]



© 2020 by the authors. Licensee MDPI, Basel, Switzerland. This article is an open access article distributed under the terms and conditions of the Creative Commons Attribution (CC BY) license (<http://creativecommons.org/licenses/by/4.0/>).